

Ferromagnetism in a dilute magnetic semiconductor — Generalized RKKY interaction and spin-wave excitations

Avinash Singh,¹ Animesh Datta,² Subrat K. Das,¹ and Vijay A. Singh¹

¹*Department of Physics, Indian Institute of Technology Kanpur - 208016*

²*Department of Electrical Engineering, Indian Institute of Technology Kanpur - 208016*

Carrier-mediated ferromagnetism in a dilute magnetic semiconductor has been studied using i) a single-impurity based generalized RKKY approach which goes beyond linear response theory, and ii) a mean-field-plus-spin-fluctuation (MF+SF) approach within a (purely fermionic) Hubbard-model representation of the magnetic impurities, which incorporates dynamical effects associated with finite frequency spin correlations in the ordered state. Due to a competition between the magnitude of the carrier spin polarization and its oscillation length scale, the ferromagnetic spin coupling is found to be optimized with respect to both hole doping concentration and impurity-carrier spin coupling energy J (or equivalently U). The ferromagnetic transition temperature T_c , determined within the spin-fluctuation theory, corresponds closely with the observed T_c values. Positional disorder of magnetic impurities causes significant stiffening of the high-energy magnon modes. We also explicitly study the stability/instability of the mean-field ferromagnetic state, which highlights the role of competing AF interactions causing spin twisting and noncollinear ferromagnetic ordering.

all theoretical studies, and we first review the emerging physical picture and the different approaches employed.

Long range ferromagnetic interaction between the $S = 5/2$ Mn^{++} ions is mediated, in the mean-field (Zener model) picture, [7–13] by a uniform itinerant-carrier spin polarization, which is caused, in turn, by an effective uniform magnetic field, resulting from site-averaging (virtual crystal approximation) of the local impurity fields. In the weak-field limit ($xJS \ll \epsilon_F$), the carrier spin polarization is proportional to the Pauli susceptibility χ_P , and the transition temperature ($T_c \sim xJ^2\chi_P$) is therefore proportional to the Mn concentration x , J^2 , the carrier effective mass m^* , and $N(\epsilon_F) \sim p^{1/3}$, where p is the hole concentration. In DMS, p is a only a small fraction (f) of x due to large compensation by As antisite defects. Therefore, the Fermi energy $\epsilon_F \sim Wp^{2/3}$ itself is quite small compared to the bandwidth W , and hence the weak-field limit is valid only for $x \ll (W/JS)^3f^2$. Valence band spin splitting comparable in size to the Fermi energy has been confirmed experimentally. [14]

Dynamical correlations in the ordered state have been studied within a path-integral formulation in which the itinerant carriers are integrated out and the effective action for the impurity spins is expanded up to quadratic order (non-interacting spin-wave approximation). [15] In contrast to the MF results, the spin stiffness (and hence T_c) is independent of J and inversely proportional to m . Other approaches incorporating dynamics include the dynamical mean field theory, [16,17] in which the local charge and spin fluctuations are included but long-range spin-wave excitations are neglected, and a RPA-level spin-fluctuation approach in which Mn disorder is treated within the coherent potential approximation (CPA). [18]

While the positional disorder of Mn ions is not taken into account in the virtual crystal approximation (VCA), several recent works highlight the importance of disorder, both positional and electronic. Stability of the collinear ferromagnetic state has been investigated with randomly distributed Mn ions, and noncollinear ordering is suggested to be common to these semiconductor systems. [19] Competing (AF) interactions leading to frustration has already been evidenced by spin-glass behavior in II-VI DMS. [20] The presence of large compensation due to As antisite defects implies substantial electronic disorder as well, and the sensitivity of T_c , magnetization M , and spin-wave spectrum to disorder has been investigated. [21–24] Monte Carlo simulations have also been used to study disorder effects on magnetic ordering; [25–27] the background fermions determine the spin interactions and

I. INTRODUCTION

The discovery of ferromagnetism in Mn-doped III-V semiconductors such as p-type $\text{In}_{1-x}\text{Mn}_x\text{As}$, [1] and $\text{Ga}_{1-x}\text{Mn}_x\text{As}$, [2] with a highest transition temperature (T_c) of 110K for Mn concentration $x = 0.053$, [3] has led to considerable interest in these dilute magnetic semiconductors (DMS). The successful search for ferromagnetic ordering above room temperature in $\text{Ga}_{1-x}\text{Mn}_x\text{N}$, [4,5] with a highest reported T_c value of 940K, [6] has added a new dimension to the interest.

Besides their potential applications in semiconductor devices such as optical isolators, magnetic sensors, non-volatile memories seamlessly integrated into semiconductor circuits etc., and possibilities in photonics and high power electronics, attention has also been focussed on the fundamental mechanism and nature of the ferromagnetic state, and the possibility of studying new magnetic cooperative phenomena such as spin-dependent tunneling, magnetoresistance, spin-dependent light emission etc. in semiconductor heterostructures arising from the new (spin) degrees of freedom.

The double-exchange model, involving the interaction $-J\vec{S}_i \cdot \vec{\sigma}_i$ between the magnetic impurity spin \vec{S}_i and the electron spin $\vec{\sigma}_i$, has been the starting point in nearly

hence the nature of the spin ordering, which in turn affects the fermionic states. Ab-Initio methods [28–31] have also been recently employed.

An alternative mechanism for the ferromagnetic coupling between impurity spins involves the hole-mediated RKKY interaction. [3] This approach is based on linear response in the weak-field limit ($J \ll \epsilon_F$), which is not quite valid for the DMS. In this paper, we present a generalized RKKY approach which takes into account the spatial variation of the impurity-induced carrier spin polarization beyond linear response theory [section II]. In the generalized RKKY picture, the local magnetic field $\vec{B}_j = J\vec{S}_j$ of a magnetic impurity at site j polarizes the electrons locally, and the mobile band electrons spread this magnetic polarization in a characteristic manner: $\vec{m}_i = \chi_{ij}(B)\vec{B}_j$, where $\chi_{ij}(B)$ represents the generalized magnetic response. The spin \vec{S}_i of another magnetic impurity placed at site i couples to this local electronic magnetization, resulting in an effective generalized RKKY spin coupling $J^2\chi_{ij}(J)\vec{S}_i \cdot \vec{S}_j$.

We find several interesting competing processes which limit the growth of spin couplings. As the RKKY response involves a particle-hole process, it vanishes for a filled (valence) band and grows with increasing hole concentration p . While the spin coupling is therefore expected to strengthen with p , a competing process involving the length scale sets in, which limits the growth of the spin coupling and therefore of the ferromagnetic transition temperature T_c . The Fermi wavelength $\lambda_F = 2\pi/k_F$, which sets the RKKY oscillation length scale, decreases with hole doping, and therefore the spin coupling between two magnetic impurities at a fixed separation goes through a maximum as a function of hole concentration [section III].

We find a similar optimization in the spin coupling as a function of the impurity field strength B . By going beyond linear response theory, and examining the generalized RKKY response for a fixed hole concentration, we find that the RKKY oscillation becomes more rapid with increasing polarizing field. Therefore, for a fixed separation between two impurity spins, the spin coupling initially increases like J^2 as expected, but then crosses over and eventually changes sign, resulting in frustration [section III]. The non-linear magnetic response thus brings out another limitation in the ferromagnetic spin coupling.

In order to determine the extent to which the magnetization response of a single impurity determines the macroscopic magnetic properties of the DMS, we have also considered a finite concentration of magnetic impurities distributed on a finite-size lattice [section IV]. Using a novel Hubbard- U representation for the magnetic impurities in a DMS, we have studied the collective magnetic response in the ferromagnetic state within a mean-field-plus-spin-fluctuation (MF+SF) approach. Treating the disorder aspects of the Mn-impurity system exactly, and electron correlation effects within the random phase approximation (RPA), our numerical analysis yields the

spin stiffness from the low-lying collective (spin-wave) excitations [section VI], which have a fundamental bearing on the ferromagnetic transition temperature T_c . Our approach also allows for a quantitative study of the stability/instability of the Hartree-Fock (mean-field) ferromagnetic state [section V], highlighting the presence of competing interactions.

II. MAGNETIC IMPURITY IN A HOST

We consider a single-band spin-fermion lattice model

$$H = \sum_{\mathbf{k},\sigma} \epsilon_{\mathbf{k}} a_{\mathbf{k},\sigma}^\dagger a_{\mathbf{k},\sigma} - \sum_i J_i \vec{S}_i \cdot \vec{\sigma}_i , \quad (1)$$

with a double-exchange interaction between the magnetic impurity spin \vec{S}_i and the electron spin $\vec{\sigma}_i$ at the impurity site i . The host (valence band) dispersion $\epsilon_{\mathbf{k}}$ is taken to be parabolic for small k (top of the band at $k = 0$), the k^2 coefficient determining the inverse carrier mass m^* . As the added holes go in long-wavelength states, the small- k particle-hole processes near the Fermi energy are dominant, and therefore other details of the energy band are expected to be relatively unimportant.

A. Host Green's function

We consider an isotropic energy-band dispersion

$$\epsilon_k = \frac{W}{2} \cos ka \quad (2)$$

in three dimensions, with the wavevector magnitude extending up to π/a . This dispersion incorporates the desired features, and yields a finite bandwidth without introducing sharp cutoffs. We choose length and energy units such that the lattice spacing $a = 1$ and the bandwidth $W = 1$. The advanced Green's function for the host is obtained as

$$\begin{aligned} g_{ij}(\omega) &= \frac{1}{N} \sum_{\mathbf{k}} \frac{e^{i\mathbf{k} \cdot (\mathbf{r}_i - \mathbf{r}_j)}}{\omega - \epsilon_{\mathbf{k}} - i\eta} \\ g_r(\omega) &= \int_0^\pi \beta(k) dk \int_0^\pi \frac{1}{2} \sin \theta d\theta \frac{e^{ikr \cos \theta}}{\omega - \epsilon_k - i\eta} \\ &= \int_0^\pi \beta(k) dk \frac{1}{\omega - \epsilon_k - i\eta} \frac{\sin kr}{kr} \end{aligned} \quad (3)$$

Here $\beta(k)$ is a k -space density of states, and for simplicity we choose a symmetric form

$$\begin{aligned} \beta(k) &= ak^2 - bk^4 & (0 \leq k \leq \pi/2) \\ &= a(k - \pi)^2 - b(k - \pi)^4 & (\pi/2 \leq k \leq \pi) , \end{aligned} \quad (4)$$

so that the usual three-dimensional k^2 form is recovered for states near both the lower and upper band edges at

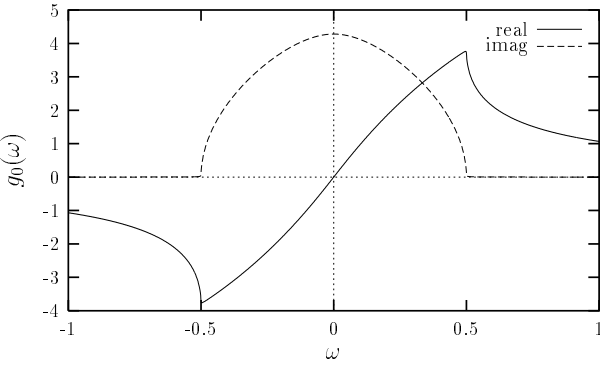


FIG. 1. Real and imaginary parts of the local host Green's function.

$k = \pi$ and $k = 0$, respectively. We choose $b = 2a/\pi^2$, so that $\beta(k)$ is smooth at $k = \pi/2$ (the slope $d\beta/dk = 0$), and an overall normalization $a = 120/7\pi^3$ so that the sum over states in the band $\int_0^\pi \beta(k) dk = 1$.

The above choice yields a symmetric band with a nearly semi-elliptical density of states, as seen in Fig. 1, showing the real and imaginary parts of the local host Green's function $g_0(\omega)$. Near the band edges, the real-part magnitude has a finite maximum and the imaginary-part has a square-root behaviour, as expected for the three-dimensional system. The band filling is shown in Fig. 2 as a function of the Fermi energy.

B. Magnetic response

We consider the impurity spin in the classical limit ($J_i \vec{S}_i \rightarrow J_i \langle \vec{S}_i \rangle = B_i \hat{z}$), and examine the magnetic response of electrons in a nearly filled band due to the magnetic coupling $-\sum_i \vec{\sigma}_i \cdot \vec{B}_i$, for an arbitrary strength of the impurity-induced local magnetic field \vec{B}_i .

For a single magnetic impurity at site j , the electronic Green's function G is exactly obtained in terms of the host Green's function g as

$$G_{ii}^\sigma(\omega) = g_{ii}(\omega) + g_{ij}(\omega) \left[\frac{-\sigma B_j}{1 + \sigma B_j g_0(\omega)} \right] g_{ji}(\omega), \quad (5)$$

where $g_0 \equiv g_{jj}$ is the local host Green's function. The resulting local magnetization m_i at site i is then obtained as

$$m_i = \int_{-\infty}^{\omega_F} \frac{d\omega}{\pi} \text{Im}[G_{ii}^\uparrow(\omega) - G_{ii}^\downarrow(\omega)], \quad (6)$$

where

$$G_{ii}^\uparrow(\omega) - G_{ii}^\downarrow(\omega) = g_{ij}(\omega) \Delta T_j g_{ji}(\omega), \quad (7)$$

in terms of the T -matrix difference

$$\Delta T_j \equiv T_j^\uparrow - T_j^\downarrow = \left[\frac{-2B_j}{1 - B_j^2 g_0^2(\omega)} \right]. \quad (8)$$

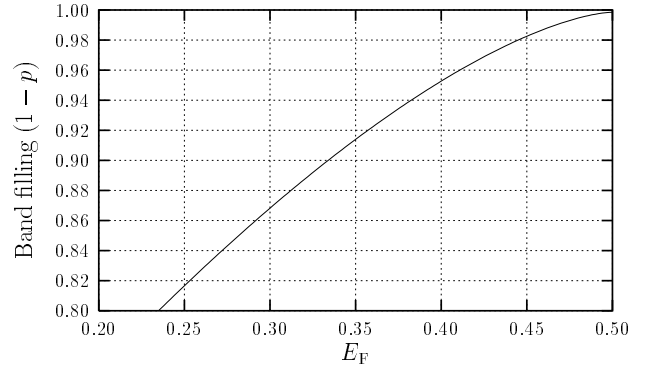


FIG. 2. Fermi-energy dependence of the band filling.

Defining a field-dependent generalized magnetic response function $\chi_{ij}(B)$ through the relation

$$m_i = \chi_{ij}(B) B_j, \quad (9)$$

Eqs. (6), (7), (8) yield

$$\chi_{ij}(B) = \int_{-\infty}^{\omega_F} \frac{d\omega}{\pi} \text{Im} \left[g_{ij}(\omega) \left(\frac{-2}{1 - B^2 g_0^2(\omega)} \right) g_{ji}(\omega) \right]. \quad (10)$$

III. EFFECTIVE SPIN COUPLINGS

Another impurity spin \vec{S}_i placed at site i will couple with the local magnetization m_i produced by the local field of the spin \vec{S}_j at site j , resulting in an effective interaction between the two spins given by

$$H_{\text{spin}}(J) = -J_i J_j \chi_{ij}(B = JS) \vec{S}_i \cdot \vec{S}_j. \quad (11)$$

A. Weak-coupling limit: RKKY interaction

When the B^2 term in Eq. (10) can be neglected (valid for $B \ll W$), one obtains a linear response

$$m_i = \chi_{ij} B_j, \quad (12)$$

where the magnetic susceptibility χ_{ij}

$$\begin{aligned} \chi_{ij} &= -2 \int_{-\infty}^{\infty} \frac{d\omega}{\pi} \text{Im}[g_{ij}(\omega) g_{ji}(\omega)] \\ &= 4 \sum_{\epsilon_l < \epsilon_F} \sum_{\epsilon_m > \epsilon_F} \frac{\phi_l^i \phi_l^{j*} \phi_m^j \phi_m^{i*}}{\epsilon_m - \epsilon_l}, \end{aligned} \quad (13)$$

yields the standard oscillating RKKY interaction

$$H_{\text{RKKY}} = -J_i J_j \chi_{ij} \vec{S}_i \cdot \vec{S}_j. \quad (14)$$

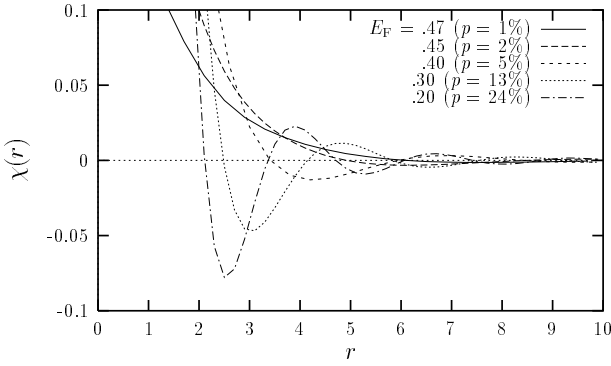


FIG. 3. Magnetic susceptibility $\chi(r)$ for different hole doping concentrations.

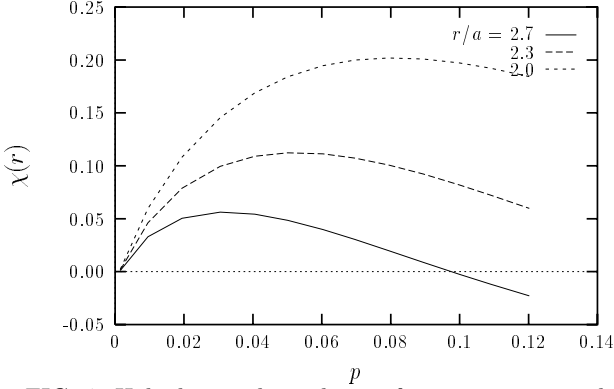


FIG. 4. Hole doping dependence of magnetic susceptibility $\chi(r)$ for different r (corresponding to average Mn-Mn separations in a cubic host lattice with 5%, 8%, and 12.5% Mn impurity concentration).

The behaviour of χ_{ij} , as a function of the separation r between the two sites i and j , shows that the oscillation becomes more rapid with doping (Fig. 3), as expected from the decreasing Fermi wavelength $\lambda_F = 2\pi/k_F$.

For a fixed separation $r/a = (1/x)^{1/3}$, corresponding to the average Mn-Mn distance in a cubic lattice with Mn concentration x , the behaviour of $\chi(r)$ is shown in Fig. 4 as a function of band filling. The ferromagnetic coupling peaks at hole concentrations about 0.6 times the Mn impurity concentration.

B. Generalized magnetic response

It appears that the conventional RKKY picture based on the weak-coupling limit ($B \ll W$) cannot provide a good description of the interaction between Mn impurities in $\text{Ga}_{1-x}\text{Mn}_x\text{As}$. Core-level photoemission [33] yields $J \sim 1$ eV, which is comparable to the host bandwidth of $W \approx 2$ eV for the heavy hole band. [34] It is therefore essential to go beyond the linear-response regime, and for $B \sim W$ we find that there are additional contributions in the generalized magnetic response func-

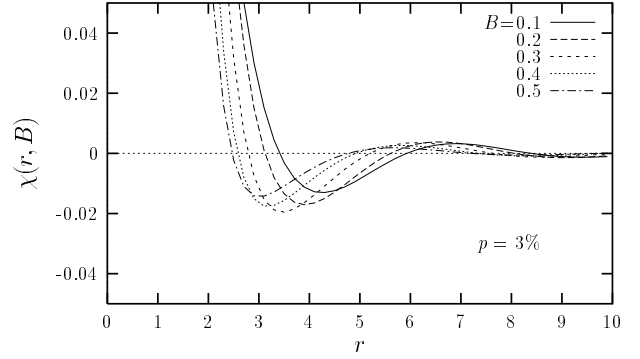


FIG. 5. The r -dependence of the generalized magnetic response $\chi(r, B)$, for different field strengths.

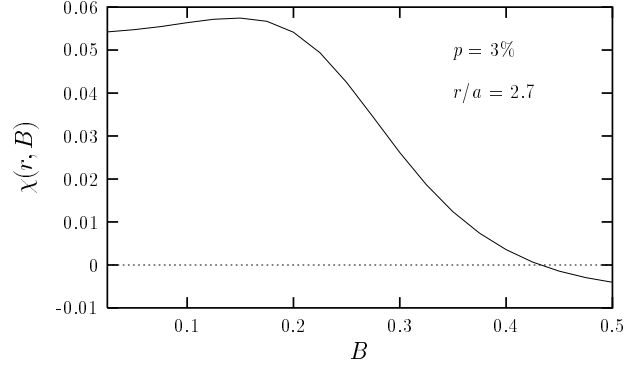


FIG. 6. The field-strength dependence of the generalized magnetic response $\chi(r, B)$, for a fixed hole concentration and Mn-Mn distance.

tion $\chi_{ij}(B)$, which qualitatively modify the nature of the magnetic response and spin couplings.

1. Impurity-state contribution

For ω outside the band ($|\omega| > W/2$), the T-matrix difference in Eq. (10) has imaginary terms of the type $\delta(\omega - \omega^*)$, arising from the two poles

$$1 \pm B g_0(\omega^*) = 0, \quad (15)$$

corresponding to a spin- \uparrow impurity state at ω_\uparrow^* (below the lower band edge), and a spin- \downarrow impurity state at ω_\downarrow^* (above the upper band edge). In three dimensions, $g_0(\omega)$ has a finite maximum at the band edges, and therefore impurity states are formed only when B exceeds a threshold strength B^* .

By expanding $g_0(\omega)$ near ω_\uparrow^* , and expressing T_j^\uparrow as a simple pole, the impurity-induced correction is given by

$$G_{ii}^\uparrow - g_{ii} = g_{ij} T_j^\uparrow g_{ji} = \frac{|\varphi_i^\uparrow|^2}{\omega - \omega_\uparrow^* - i\eta}, \quad (16)$$

where the impurity-state wavefunction φ_i^\uparrow is given by

$$\varphi_i^\uparrow = \frac{g_{ij}(\omega = \omega_{\uparrow}^*)}{\sqrt{-dg_0/d\omega|_{\omega=\omega_{\uparrow}^*}}}.$$
 (17)

For any finite doping, only the spin- \uparrow impurity state is occupied, and the impurity-state contribution to the local magnetization is therefore simply obtained as

$$m_i^* = |\varphi_i|^2.$$
 (18)

With increasing B , the impurity-state wavefunction becomes more localized, and $\varphi_i \rightarrow \delta_{ij}$ as $B \rightarrow \infty$.

2. Band contribution

The other contributions to the imaginary part in Eq. (10) are from within the band ($|\omega| < W/2$), and involve the real (imaginary) part of $\Delta T_j(\omega)$ and imaginary (real) part of $g_{ij}(\omega)g_{ji}(\omega)$.

Including both the band and impurity contributions, the generalized magnetic response $\chi(r, B)$ evaluated from Eq. (10) is shown in Fig. 5 for different field strengths. The length scale at which the first crossover from ferromagnetic to antiferromagnetic coupling takes place is seen to decrease with increasing B . Fig. 6 shows the generalized magnetic response $\chi(r, B)$, for a fixed hole concentration and Mn-Mn distance. For small $B = JS$, the response is essentially constant (linear response), and in this regime the generalized RKKY interaction energy $B^2\chi(r, B)$ grows like J^2 , as in the mean-field and conventional RKKY pictures. However, the sharp suppression in the generalized magnetic response for $B/W > 0.2$ limits this growth and leads to a peak, which is seen to shift to higher B values with decreasing Mn-Mn separation (Fig. 7). This effect significantly increases the spin coupling in a higher Mn concentration system (such as GaMnN) beyond the factor expected from the spin response (Fig. 4).

As the effective carrier mass m^* scales like the inverse bandwidth $1/W$, the m^* dependence of the generalized magnetic response $\chi(r, B)$ can be directly deduced from Fig. 6, showing the $B/W \propto m^*$ dependence for a fixed $B = JS$. The magnetic response in the (fixed) unit of $1/B$ is obtained by multiplying $\chi(r, B)$ in Fig. 6 (in unit of $1/W$) by B/W . This yields a linear m^* dependence of $\chi(r, B)$ (and hence the spin coupling energy and T_c) for low effective mass and then a sharp suppression with increasing m^* . Sublinear dependence of T_c at large m^* has also been reported in Monte Carlo studies. [25]

For a nominal host bandwidth of 10 eV (with $1 \text{ eV} \approx 10^4 \text{ K}$), the peak interaction energies are about 250 K, 600 K and 1400 K for Mn concentrations of 5%, 8%, and 12.5%, and hole concentrations of 3%, 5%, and 8%, respectively [Fig. 7]. From this spin interaction energy $(JS)^2\chi$, the ferromagnetic transition temperature

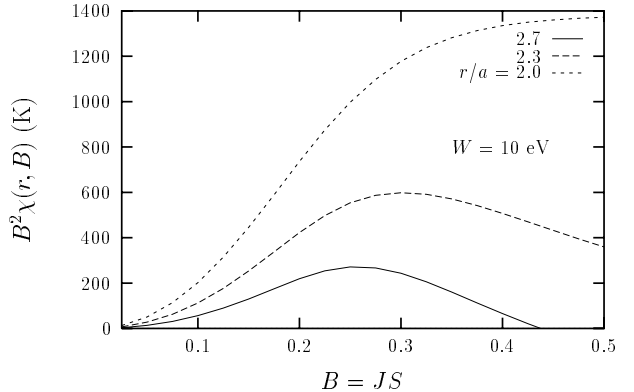


FIG. 7. The generalized RKKY interaction energy $B^2\chi(r, B)$ as a function of the local field strength B , for different Mn-Mn distances. The host bandwidth is nominally taken as 10 eV.

T_c can be estimated within the spin-fluctuation theory. For a nearest-neighbour quantum Heisenberg model (interaction energy \mathcal{J}) on a hypercubic lattice (coordination number z), the transition temperature is given by $T_c = T_c^{\text{MF}}/f_{\text{sf}}$, somewhat lower than the mean-field value $T_c^{\text{MF}} = \mathcal{J}S(S+1)z/2$. [35] Here $f_{\text{sf}} = (1/N)\sum_{\mathbf{k}}(1 - \gamma_{\mathbf{k}})^{-1} \gtrsim 1$ is a geometrical spin-fluctuation factor, where $\gamma_{\mathbf{k}} \equiv (\cos k_x + \cos k_y + \cos k_z)/3$ in three dimensions.

As the effective RKKY interaction term between two spins is $J^2\chi_{ij}\vec{S}_i \cdot \vec{S}_j$, we take $\mathcal{J} = J^2\chi$ and obtain $T_c \approx 3(JS)^2\chi$ for $z = 6$. Taking a realistic bandwidth of $W = 2 \text{ eV}$ for the heavy valence band, [34] the peak energy in Fig. 7 translates to a peak T_c of about 150 K and 850 K for 5% and 12.5% Mn concentrations, quite close to the observed highest T_c values for $\text{Ga}_{1-x}\text{Mn}_x\text{As}$ and $\text{Ga}_{1-x}\text{Mn}_x\text{N}$.

IV. HUBBARD- U REPRESENTATION OF MAGNETIC IMPURITIES

We now consider a (purely fermionic) Hubbard-model representation for the randomly distributed magnetic impurities on a cubic lattice:

$$H = t \sum_{\langle ij \rangle \sigma} \left(\hat{a}_{i\sigma}^\dagger \hat{a}_{j\sigma} + \text{h.c.} \right) + t' \sum_{\langle Ij \rangle \sigma} \left(\hat{a}_{I\sigma}^\dagger \hat{a}_{j\sigma} + \text{h.c.} \right) + \epsilon_d \sum_{I,\sigma} \hat{a}_{I\sigma}^\dagger \hat{a}_{I\sigma} + U \sum_I (\hat{n}_{I\uparrow} - n_I)(\hat{n}_{I\downarrow} - n_I), \quad (19)$$

where I refers to the impurity sites, ϵ_d is the impurity on-site energy and $n_I = \langle \hat{n}_{I\uparrow} + \hat{n}_{I\downarrow} \rangle/2$ is the spin-averaged impurity charge density. Higher spin magnetic impurities, such as the $S = 5/2$ Mn impurities in $\text{Ga}_{1-x}\text{Mn}_x\text{As}$, can be realistically represented within a generalized Hubbard model representation involving multiple orbitals and different interaction processes (direct and exchange

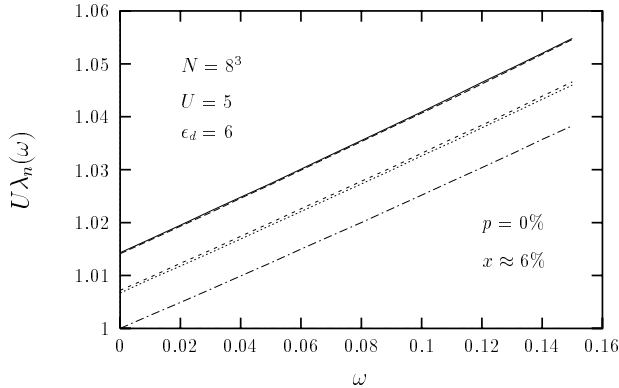


FIG. 8. Instability of the undoped (HF) ferromagnetic state. The Goldstone mode ($U\lambda_G = 1$) corresponds to the minimum eigenvalue of the $[\chi^0(\omega = 0)]$ matrix, indicating maximal instability.

type, with respect to orbital indices). [36] For simplicity, we have taken the same hopping ($t' = t$) between the host-host and host-impurity nearest-neighbour pairs of sites. The energy-scale origin is set so that the host on-site energy is zero. The form of the Hubbard interaction term is such that in the Hartree-Fock approximation it reduces to the double-exchange term.

A. Hartree-Fock ferromagnetic state

In the Hartree-Fock (mean-field) approximation, the interaction term reduces to a magnetic coupling of the electron to the local mean (magnetic) field $\vec{\Delta}_I$:

$$H_{\text{int}}^{\text{HF}} = - \sum_I \vec{\sigma}_I \cdot \vec{\Delta}_I, \quad (20)$$

where the electronic spin operator $\vec{\sigma}_I = \Psi_I^\dagger [\vec{\sigma}] \Psi_I$ in terms of the spinor $\Psi_I = \begin{pmatrix} \hat{a}_{I\uparrow} \\ \hat{a}_{I\downarrow} \end{pmatrix}$, and the mean field $\vec{\Delta}_I$ is self-consistently determined from the ground-state expectation value:

$$2\vec{\Delta}_I = U \langle \vec{\sigma}_I \rangle. \quad (21)$$

Thus, in the classical (Hartree-Fock) limit, the interaction term reduces to the corresponding form of the double-exchange term, with the mean field $\vec{\Delta}_I$ representing the impurity-induced local magnetic field \vec{B}_I .

B. Stability of the HF state

The self-consistent, HF ferromagnetic state, with all local moments aligned in the same symmetry-breaking

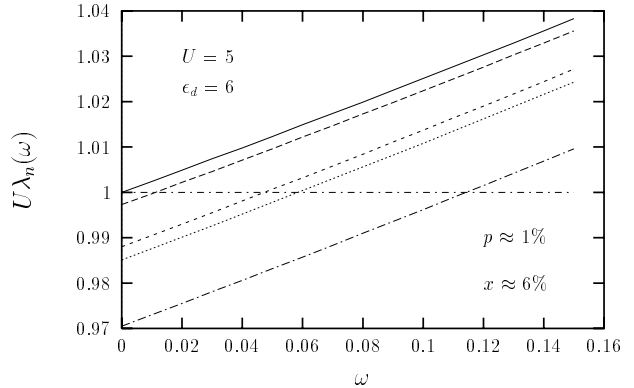


FIG. 9. Stabilization of the ferromagnetic state with hole doping; the Goldstone mode now corresponds to the maximum eigenvalue.

direction, does not necessarily represent a stable (lowest-energy) state. This is because the HF state really represents an energy extremum, which may correspond to a saddle point having local energy minimum and maximum along different directions in the order-parameter space. The stability of the HF state with respect to transverse perturbations in the order parameter is indicated by the maximum eigenvalue λ_{max} of the $[\chi^0(\omega = 0)]$ matrix (Eq. 24). [37] The HF state is stable if $U\lambda_{\text{max}} = 1$, corresponding to the massless Goldstone mode, representing a rigid rotation of the ordering direction. Instability is indicated if $U\lambda_{\text{max}} > 1$, signalling a growth of transverse perturbations about the HF state, which can also be interpreted as negative-energy bosonic modes.

Figure 8 shows some of the eigenvalues of the $[\chi^0(\omega)]$ matrix (including the minimum and maximum) for the undoped HF ferromagnetic state of an 8^3 system, with a semi-ordered arrangement of 32 magnetic impurities (see section V for details). For $\omega = 0$, the Goldstone mode ($U\lambda_G = 1$) is seen to correspond to the *lowest eigenvalue*, indicating maximal instability of the ferromagnetic state. The structure of the eigenvector corresponding to the maximum eigenvalue indicates a tendency towards AF ordering of the impurity spins. The AF coupling arises from the exchange interaction $J' \sim t'^2/U$ due to the effective hopping t' (associated with impurity-band formation) between impurity sites. In the absence of the hole-induced (RKKY) ferromagnetic coupling, this exchange interaction dominates and favours AF ordering of impurity spins. With hole doping, the ferromagnetic state gets stabilized, and the Goldstone mode now corresponds to the maximum eigenvalue (Fig. 9).

C. Spin wave excitations

Transverse spin fluctuations are gapless, low-energy excitations in the broken-symmetry state of magnetic systems possessing continuous spin-rotational symmetry.

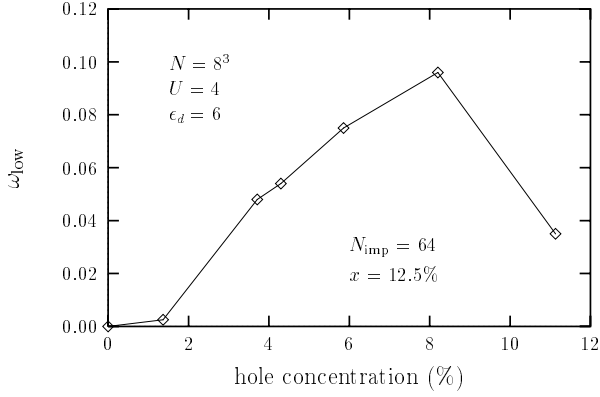


FIG. 10. Hole doping dependence of the lowest magnon mode energy for an ordered impurity arrangement, showing a steep decrease in the spin stiffness after the initial rise.

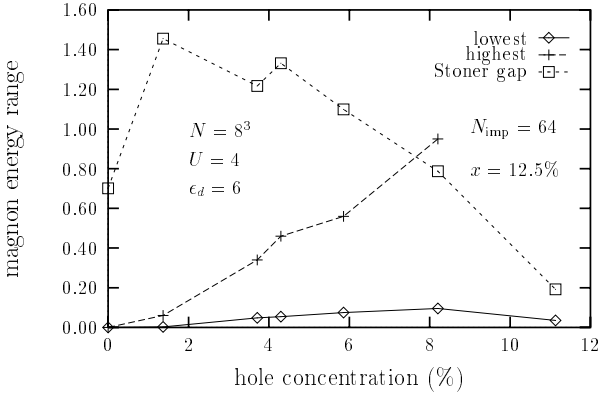


FIG. 11. Hole doping dependence of the lowest and highest magnon energies, along with the Stoner gap.

Therefore, at low temperatures they play an important role in diverse macroscopic properties such as existence of long-range order, magnitude and temperature dependence of the order parameter, magnetic transition temperatures, spin correlations etc.

We study the time-ordered, transverse spin (magnon) propagator involving the spin-lowering (S_i^-) and spin-raising (S_i^+) operators at sites i and j :

$$\chi_{ij}(t - t') = \langle \Psi_G | T[S_i^-(t)S_j^+(t')] | \Psi_G \rangle. \quad (22)$$

At the RPA level, the magnon propagator in frequency space is given by

$$[\chi^{-+}(\omega)] = \frac{[\chi^0(\omega)]}{1 - [U][\chi^0(\omega)]}, \quad (23)$$

where the zeroth-order, antiparallel-spin particle-hole propagator

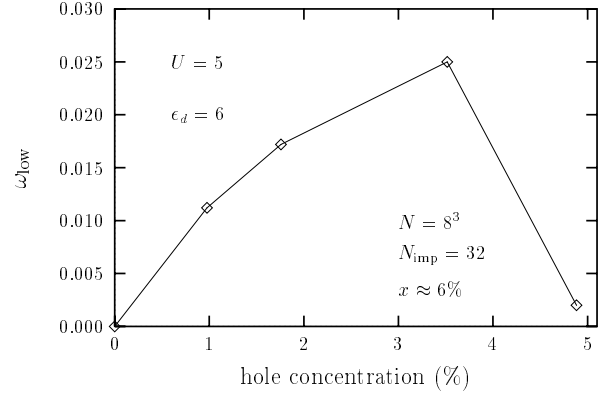


FIG. 12. Hole doping dependence of the lowest magnon energy, involving the relatively softer planar spin couplings due to greater in-plane impurity separation.

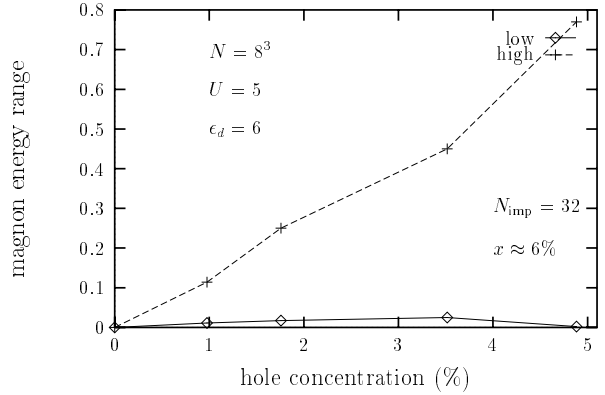


FIG. 13. Hole doping dependence of the magnon energy range for the semi-ordered impurity arrangement.

$$\begin{aligned} [\chi^0(\omega)]_{ij} &= i \int \frac{d\omega'}{2\pi} G_{ij}^\uparrow(\omega') G_{ji}^\downarrow(\omega' - \omega) \\ &= \sum_{\substack{E_m > E_F \\ E_l < E_F}} \left(\frac{\phi_{l\uparrow}^i \phi_{m\downarrow}^j \phi_{m\downarrow}^j \phi_{l\uparrow}^j}{E_{m\downarrow} - E_{l\uparrow} + \omega} + \frac{\phi_{l\downarrow}^i \phi_{m\uparrow}^j \phi_{m\uparrow}^j \phi_{l\downarrow}^j}{E_{m\uparrow} - E_{l\downarrow} - \omega} \right) \end{aligned} \quad (24)$$

is evaluated using the eigenvalues $E_{l\sigma}$ and eigenvectors $\phi_{l\sigma}$ in the self-consistent, broken-symmetry state. In Eq. (23), the diagonal interaction matrix $[U]_{ii} = U\delta_{ii}$ has non-vanishing elements only at the magnetic impurity sites. For site-dependent interactions, it is convenient to recast Eq. (23) using simple matrix manipulations:

$$[\chi^{-+}(\omega)] = \frac{1}{[A(\omega)]} - \frac{1}{[U]}, \quad (25)$$

where $[A(\omega)] = [U] - [U][\chi^0(\omega)][U]$ is a symmetric matrix, having non-vanishing matrix elements only in the reduced impurity basis:

$$[A(\omega)]_{IJ} = U(1 - U[\chi^0(\omega)]_{IJ}). \quad (26)$$

Magnon modes, represented by the poles in the transverse spin propagator $[\chi^{-+}(\omega)]$, are hence given by the poles of the matrix $[A(\omega)]_{IJ}$, as $[U]$ is non-singular. In

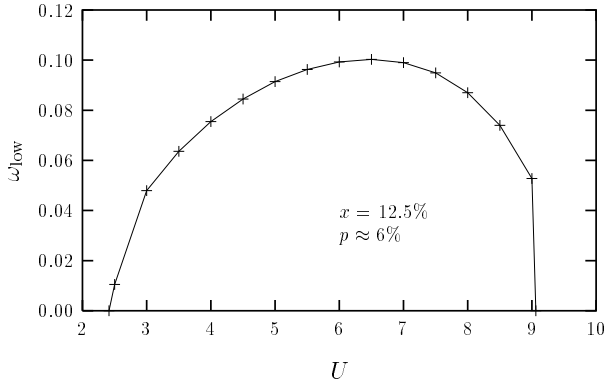


FIG. 14. U -dependence of the lowest magnon mode energy for an ordered impurity arrangement, with $N_{\text{imp}} = 64$ and $N_{\uparrow} = 482$.

terms of the eigenvalues λ_n and eigenvectors φ_n of the $[\chi^0(\omega)]_{IJ}$ matrix, the magnon energies ω_n are therefore given by

$$1 - U\lambda_n(\omega_n) = 0. \quad (27)$$

V. MAGNON ENERGIES AND SPIN STIFFNESS IN THE FERROMAGNETIC STATE

The spin couplings and stiffness in the ferromagnetic state can be determined from the magnon energies. To see how the magnitude and sign of the spin couplings depend on impurity separation, we have considered ordered, semi-ordered, and disordered arrangements of magnetic impurities, taking a cubic host lattice with $N = 8^3 = 512$ sites. We first study the ordered arrangement of 64 magnetic impurities on a (cubic) superlattice with a spacing of $2a$, corresponding to an overall impurity concentration of 1/8. For the undoped (insulating) state with filled valence bands, $N_{\uparrow} = 512$ and $N_{\downarrow} = 512 - 64 = 448$, so that the 64 spin- \downarrow impurity states (pushed up by the local mean field) are unoccupied, resulting in the local moments on the magnetic sites. Hole doping is introduced by reducing N_{\uparrow} , and band fillings so chosen that the Fermi energy lies in gaps between degenerate groups of eigenvalues.

The undoped self-consistent ferromagnetic state is found to be maximally unstable, as discussed earlier. Indeed, the self-consistent antiferromagnetic state is actually found to be stable, confirming the dominance of the AF spin couplings $J' \sim t'^2/U$. With hole doping, the ferromagnetic state is stabilized, and the magnon energies ω_n are extracted from the pole condition $U\lambda_n(\omega_n) = 1$. Hole doping dependence of the lowest magnon energy ω_{low} is shown in Fig. 10. The full range of magnon energies lies within the Stoner gap for low doping (Fig. 11), the highest-energy mode merging with Stoner excitations at about 8% hole concentration. This magnon

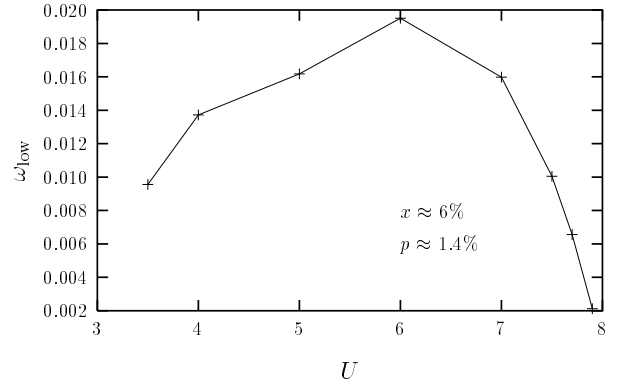


FIG. 15. U -dependence of the lowest magnon mode energy for a disordered impurity arrangement, with $N_{\text{imp}} = 30$ and $N_{\uparrow} = 505$.

energy range allows the spin couplings to be extracted, as discussed below.

Assuming nearest-neighbour exchange interaction J between the impurity spins on the superlattice, the spin-wave energies are given by

$$\omega_{\mathbf{q}} = JSz(1 - \gamma_{\mathbf{q}}), \quad (28)$$

where $\gamma_{\mathbf{q}} = (\cos q_x + \cos q_y + \cos q_z)/3$. The magnon modes on the impurity superlattice are plane waves, with wave-vector components given by $q_{\mu} = n_{\mu}2\pi/L$, where n_{μ} are integers and $L = 4$ for the 64-impurity superlattice. The wave vectors $\mathbf{q} = (1, 0, 0)2\pi/L$ etc. and $\mathbf{q} = (2, 2, 2)2\pi/L$ correspond to the lowest- and highest-energy modes, respectively. The corresponding energies $\omega_{\text{low}} = JSz/3$ and $\omega_{\text{high}} = 2JSz$ yield a ratio $\omega_{\text{high}}/\omega_{\text{low}} = 6$. We not only find the actual ratio to be quite close (about 7 for most doping cases), but the degeneracies in the magnon-energy spectrum are also in close agreement, indicating that nearest-neighbour spin coupling is dominant.

We next consider a more dilute system with a semi-ordered arrangement of 32 impurities in the 8^3 lattice ($x \approx 6\%$), such that the impurity separation is $2a$ in the z direction and $\sqrt{8}a$ in the xy plane. The hole-doping dependence of the lowest and highest magnon energies are shown in Figs. 12 and 13. The lowest magnon energy, involving the relatively softer planar spin coupling, is seen to decrease sharply with hole concentration after the initial rise, very similar to the behaviour in Fig. 10. This doping behaviour is qualitatively similar to that of the RKKY spin coupling $J^2\chi$ (Fig. 4). Furthermore, comparison of Figs. 10 and 12 directly shows the magnon softening due to increased spin separation. The highest magnon energy, however, is seen to be enhanced by disorder, for the same hole concentration (see Figs. 11 and 13).

Figure 14 shows the U -dependence of the lowest magnon energy, revealing an optimization in the ferromagnetic spin coupling with respect to the interaction

energy U . As the local mean (magnetic) field $\Delta_I \sim U$ (Eq. 21), the interaction energy U plays the role of the local field B in the RKKY analysis. In terms of the host bandwidth $W = 12t$, the peak in the spin coupling energy occurs at $U/W \approx 1/2$, and comparison with Fig. 7 again shows a striking similarity with the RKKY picture. A similar behaviour is seen for a disordered arrangement (Fig. 15), with impurity separations ranging between 2 and 3. The discontinuous transition seen in Fig. 14 appears to be intrinsic to the ordered impurity arrangement.

VI. CONCLUSIONS

A comparative study of a generalized RKKY approach and a MF+SF approach offers new and useful insight into the mechanism of ferromagnetic ordering in a dilute magnetic semiconductor. In the RKKY picture, the ferromagnetic spin coupling is mediated by the impurity-induced oscillating carrier spin polarization. The competition between the increasing magnitude of spin polarization and the increasing rapidity of the RKKY oscillation with hole doping results in an optimum hole concentration ($p \approx 0.6x$) for maximum spin coupling. Another optimization involving the exchange coupling J is revealed by going beyond linear response (generalized RKKY). After the initial J^2 rise, the effective impurity spin coupling $J^2\chi(r, J)$ peaks at $JS/W \approx 0.3$ (for $x \sim 5\%$) and then decreases rapidly with J . The ferromagnetic transition temperature T_c , determined within the spin-fluctuation theory from the spin coupling energy for a realistic (heavy) hole bandwidth, corresponds closely with the observed T_c values in $\text{Ga}_{1-x}\text{Mn}_x\text{As}$ and $\text{Ga}_{1-x}\text{Mn}_x\text{N}$. With appropriate hole doping, transition temperature much above room temperature appears possible for $x = 1/8$, which is within experimental limit. [38]

These features of the generalized RKKY picture survive at finite impurity concentration, studied within a MF+SF approach using a novel Hubbard- U representation of the magnetic impurities in a DMS. Dynamical effects associated with finite-frequency spin correlations are included in this approach, which also allows for a stability analysis of the MF ferromagnetic state, highlighting the role of competing AF interactions leading to spin twisting and noncollinear ferromagnetic ordering. The observed optimization of the magnon energy ω_{low} with respect to both hole doping and interaction strength U follow the single-impurity based RKKY results, and are also in qualitative agreement with Monte Carlo investigations of a single-band model. [27] For a fixed J/W or U/W , both the spin coupling energy $J^2\chi(r, J)$ and the magnon energy scale like the carrier bandwidth W .

Several new features do emerge at a finite impurity concentration. A simple analysis for the effective carrier mass dependence ($m^* \propto 1/W$) of the magnon energy ω/U (converted from ω/t in Figs. 14 and 15)

yields a nearly constant behaviour for intermediate m^* ($1/3 \lesssim U/W \lesssim 1/2$), falling off to zero on either sides. On the other hand, the spin coupling energy (for a fixed J) increases linearly for low m^* and then falls off to zero at large m^* . We also find that the magnon energy is smaller (roughly by factor of 4) than the corresponding magnon mode energy estimated from the RKKY spin coupling energy. This reduction is presumably due to a suppression of the magnetization response $\chi(r, B)$ in the presence of a Zeeman splitting of the two spin bands. In contrast, impurity disorder substantially enhances the magnon mode energies. Figures 11 and 13 show that for the same hole concentration, ω_{high} for the semi-ordered impurity arrangement is nearly double that for the ordered case. This enhancement is even more dramatic for a more disordered arrangement of 27 impurities (with NN impurity separations of 2 or 3 in all three directions). A nearly stable non-homogeneous ferromagnetic state, with vanishing local moments on a finite fraction of the impurity sites, is also found for this disorder case.

A distribution in spin couplings, with weak and strong bonds, has been suggested to be responsible for anomalous temperature dependence of magnetization, susceptibility, specific heat etc. [39] Within our Hubbard model approach, the spin couplings $J(r) \sim U^2\chi^0(r)$ in the magnetic state [40] can be determined from the $[\chi^0]_{IJ}$ matrix in the reduced impurity basis. A detailed study of the distribution of $J(r)$ for different (Mn) disorder realizations and the magnon energy spectrum is currently in progress.

ACKNOWLEDGEMENT

Helpful discussions with T. Pareek and R. C. Budhani are gratefully acknowledged.

¹ H. Ohno, H. Munekata, T. Penny, S. von Molnar, and L. L. Chang, Phys. Rev. Lett. **68**, 2664 (1992).
² H. Ohno, A. Shen, F. Matsukara, A. Oiwa, A. Endo, S. Katsumoto, and Y. Iye, Appl. Phys. Lett. **69**, 363 (1996).
³ F. Matsukara, H. Ohno, A. Shen, and Y. Sugawara, Phys. Rev. B **57**, R2037 (1998).
⁴ N. Theodoropolpu *et al.*, Appl. Phys. Lett. **78**, 3475 (2001).
⁵ M. L. Reed *et al.*, Appl. Phys. Lett. **79**, 3473 (2001).
⁶ S. Sonoda *et al.*, J. Cryst. Growth **237-239**, 1358 (2002).
⁷ T. Dietl, A. Haury, and Y. M. d'Aubigne, Phys. Rev. B **55**, R3347 (1997).
⁸ M. Takahashi, Phys. Rev. B **56**, 7389 (1997).
⁹ T. Jungwirth, W. A. Atkinson, B. H. Lee, and A. H. MacDonald, Phys. Rev. B **59**, 9818 (1999); B. H. Lee, T. Jungwirth, and A. H. MacDonald, *ibid* **61**, 15606 (2000).

¹⁰ T. Dietl, H. Ohno, F. Matsukara, J. Cibert, and D. Ferrand, *Science*, **287**, 1019 (2000).

¹¹ T. Dietl, H. Ohno, and F. Matsukara, cond-mat/007190 (unpublished).

¹² T. Dietl, F. Matsukara, and H. Ohno, *Phys. Rev. B* **66**, 033203 (2002).

¹³ T. Jungwirth, J. König, J. Sinova, K. Kučera, and A. H. MacDonald, *Phys. Rev. B* **66**, 012402 (2002).

¹⁴ H. Ohno, N. Akiba, F. Matsukara, A. Shen, K. Ohtani, and Y. Ohno, *Appl. Phys. Lett.* **73**, 363 (1998).

¹⁵ J. König, H. H. Lin, and A. H. MacDonald, *Phys. Rev. Lett.* **84**, 5628 (2000); J. König, T. Jungwirth, and A. H. MacDonald, *Phys. Rev. B* **64**, 184423 (2001).

¹⁶ A. Chattopadhyay, S. Das Sarma, and A. J. Millis, *Phys. Rev. Lett.* **87**, 227202 (2001).

¹⁷ S. Das Sarma, E. H. Hwang, and A. Kaminski, cond-mat/0211496 (2002).

¹⁸ G. Bouzerar and T. P. Pareek, *Phys. Rev. B* **65**, 153203 (2002).

¹⁹ J. Schliemann and A. H. MacDonald, *Phys. Rev. Lett.* **88**, 137201 (2002).

²⁰ J. K. Furdyna and J. Kossut, *Semiconductors and Semimetals*, Vol. 25 (Academic Press, New York, 1988).

²¹ M. Berciu and R. N. Bhatt, *Phys. Rev. Lett.* **87**, 107203 (2001).

²² A. L. Chudnovskiy and D. Pfannkuche, *Phys. Rev. B* **65**, 165216 (2002).

²³ M. Berciu and R. N. Bhatt, *Phys. Rev. B* **66**, 085207 (2002).

²⁴ G. Bouzerar, J. Kudrnovský, and P. Bruno, cond-mat/0208596 (2002).

²⁵ J. Schliemann, J. König, and A. H. MacDonald, *Phys. Rev. B* **64**, 165201 (2001).

²⁶ M. P. Kennett, M. Berciu and R. N. Bhatt, *Phys. Rev. B* **66**, 045207 (2002).

²⁷ G. Alvarez, M. Mayr, and E. Dagotto, *Phys. Rev. Lett.* **89**, 277202 (2002).

²⁸ H. Akai, *Phys. Rev. Lett.* **81**, 3002 (1998).

²⁹ M. Shirai *et al.*, *J. Magn. Magn. Mater.* **177-181**, 1383 (1998).

³⁰ S. Sanvito, P. Ordejón, and N. A. Hill, *Phys. Rev. B* **63**, 165206 (2001).

³¹ L. M. Sandratskii and P. Bruno, *Phys. Rev. B* **66**, 134435 (2002).

³² L. Craco, M. S. Laad, and E. Müller-Hartmann, cond-mat/030342 (2003).

³³ J. Okabayashi *et al.*, *Phys. Rev. B* **58**, R4211 (1998).

³⁴ J. R. Chelikowski and M. L. Cohen, *Phys. Rev. B* **14**, 556 (1976); W. A. Harrison, *Electronic Structure and the Properties of Solids* (Freeman, San Francisco, 1980).

³⁵ S. Doniach and E. H. Sondheimer, *Green's Functions for Solid State Physicists* (Benjamin, New York, 1974).

³⁶ A. Singh and P. Sen, *Phys. Rev. B* **57**, 10598 (1998).

³⁷ For a stability analysis of the hole and electron doped antiferromagnetic state, see A. Singh and Z. Tešanović, *Phys. Rev. B* **41**, 614 (1990); A. Singh and H. Ghosh, *Phys. Rev. B* **65**, 134414 (2002).

³⁸ A. J. Blattner and B. W. Wessels, cond-mat/0205602 (2002).

³⁹ M. P. Kennett, M. Berciu and R. N. Bhatt, *Phys. Rev. B* **65**, 115308 (2002).

⁴⁰ A. Singh, *Phys. Rev. B* **48**, 6668 (1993).